AD-A122 326 LOW VOLTAGE FREE ELECTRON LASER OPTICS - FIRST STAGE DESIGN(U) SCHAFER (W J) ASSOCIATES INC WAKEFIELD MA 17 NOV 82 WJSA-FTR-82-209 N000014-80-C-0518 1/1

UNCLASSIFIED F/G 20/5 NL

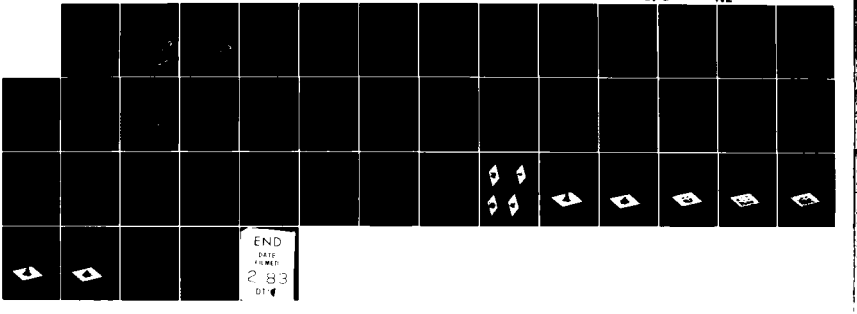

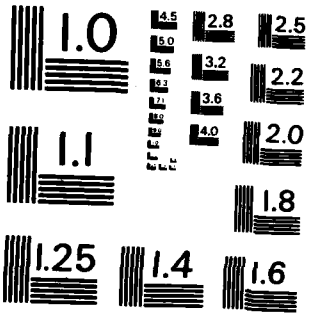

(2)

WJSA-FTR-82-209

LOW VOLTAGE FREE ELECTRON LASER OPTICS - FIRST STAGE DESIGN

17 November 1982

Contract Number: N00014-80-C-0515

Prepared for:

PCO - Office of Naval Research
Department of the Navy
800 N. Quincy Street
Arlington, VA 22217

Prepared by:

W. J. Schafer Associates, Inc.
10 Lakeside Office Park
Wakefield, MA 01880

WJSA-FTR-82-209

LOW VOLTAGE FREE ELECTRON LASER OPTICS - FIRST STAGE DESIGN

17 November 1982

Contract Number: N00014-80-C-0515

Prepared for:

PCO - Office of Naval Research
Department of the Navy
800 N. Quincy Street
Arlington, VA 22217

Prepared by:

W. J. Schafer Associates, Inc.
10 Lakeside Office Park
Wakefield, MA 01880

TABLE OF CONTENTS

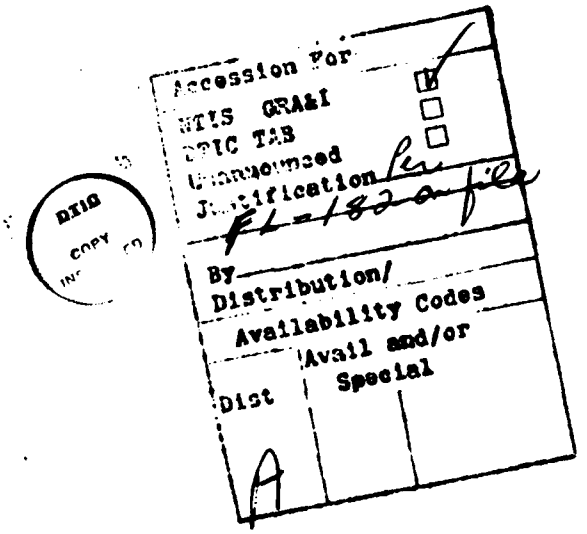

LIST OF TABLES

LIST OF FIGURES

LIST OF FIGURES (Continued)

I. INTRODUCTION

The concept of the two stage free electron laser was advanced by Elias[1] as well as others about four years ago. In the two stage free electron laser, a conventional magnetostatic wiggler is used to generate radiation in the far infrared or submillimeter range; and this radiation is used as a pump to produce electromagnetic radiation in the visible or UV. The advantage of this concept lies chiefly in the use of low energy electrons ($\lesssim$ 10 MeV) whose energy can be recovered very efficiently after FEL interaction. In our last study[2], we investigated several methods of reducing electromagnetic pump optical cavity losses. The general design considerations for a two-stage free electron laser were given. A point design for the proposed UCSB experiment was given.

In this study, we have tried to validate the earlier point design with actual electron dynamics calculations. We find the agreement between the exact one-dimensional code and the point design parameters to be satisfactory. The calculations are carried out for the first stage interaction only. We have also developed a program to calculate the transverse mode structure of the pump radiation in the cavity. This will be used in future calculations for assessing the performance of the second stage of the FEL. In Section II, we have summarized the results of design and code verification. In Section III, we discuss the transverse mode structure. Section IV contains a summary of the results so far obtained.

II. ELEMENTARY CONSIDERATIONS

A conceptual design of the first stage FEL cavity was carried out previously. This involved compromising on the gain, saturation flux etc. High gain usually implies low saturation flux and vice versa. One needs high gain to start the first stage FEL quickly, but at the same time one also needs high saturation flux since that will be the pump field for the second stage. In this section we shall first briefly go through some of the scaling relations that determine the wiggler parameters. These have been described in detail before[2]. Having chosen a set of design parameters, we shall describe the electrodynamics code that actually solves for the gain of the FEL.

We shall first assume that the first stage wiggler is made out of $SmCO_5$ permanent magnet as shown in Figure 1. For a magnet bar height $g = 3\,\lambda_w/8$ and a fill factor of unity, i.e. no gaps between neighboring magnets, the normalized wiggler vector potential on axis can be written[3]

$$a_w = 1.07 \times 10^{-4}\, B_r \lambda_w \exp\left[-2\pi\, h/\lambda_w\right] \qquad (2.1)$$

where B_r is the remnant field in gauss and other quantities are defined in Figure 1.

The photon beam width at the entrance to the wiggler is denoted by 2w and for reasonable clearance the magnet separation 2h can be taken to be at least a factor of α larger than 2w. The Rayleigh range Z_R is related to the photon beam waist radius w_o by

$$Z_R = \pi\, w_o^2/\lambda \qquad (2.2)$$

The length of the wiggler L_W is taken to be 2 q times the Rayleigh range. Thus the beam radius at the entrance to the wiggler can be written as

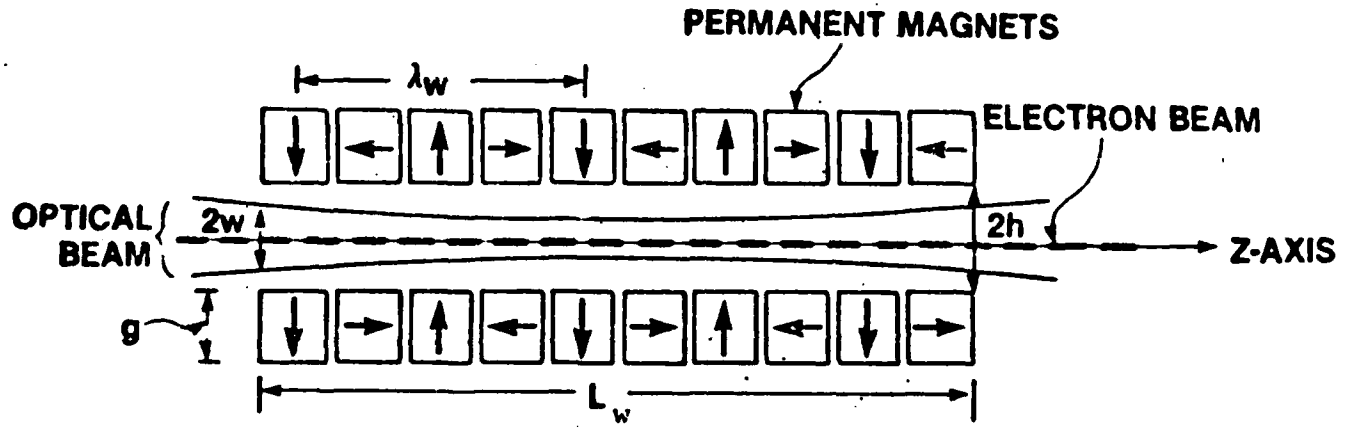

Figure 1. Geometry of the Permanent Magnet Wiggler for Optimization (From Ref. 3)

$$w = w_o \left[1+(L_w/2Z_R)\right]^{1/2} = \left[\lambda Z_r (1+q^2)/\pi\right]^{1/2} \quad (2.3)$$

Replacing h in equation (2.1) by αw and substituting (2.3) we get,

$$a_w = 1.07 \times 10^{-4} B_r \lambda_w \exp\left[-2\pi\alpha \left[\lambda Z_R(1+q^2)/\pi\right]^{1/2}/\lambda_w\right] \quad (2.4)$$

The output wavelength λ is related to λ_w and a_w through

$$\lambda = \lambda_w (1 + a_w^2)/2\gamma^2 \quad (2.5)$$

The two convenient sets of independent parameters are λ_w and Z_R and we shall plot the different physical quantities in maps with λ_w and Z_R as axes. Figure 2 shows a plot of constant a_w lines. In plotting the figure, we had to assume a value for γ. The γ that can be obtained for the UCSB experiment is 12 and we have taken that to be a fixed value. Changing γ would result in similar plots.

The small signal gain $g_o L_w$ per pass is given by [4]

$$g_o L_w = \frac{2}{\pi} \frac{1}{\sqrt{e\pi}} \frac{r_o^2 n_e}{mc^2} \frac{B^2\lambda_w^2}{(1 + a_w^2)^{3/2}} \frac{\lambda^{3/2}}{\lambda_w^{1/2}} \frac{L_w}{(\Delta\upsilon/\upsilon)^2} \quad (2.6)$$

where r_o is the classical electron radius, n_e is the electron density in the beam and $(\Delta\upsilon/\upsilon)$ is the fractional line width and is taken to be ~ 1/2N (N being the number of wiggler periods). In Ref. 2, Eq. (4.6) the factor $(1+a_w^2)^{3/2}$ has been mistyped as $(1+a_w^2)^{1/2}$. If we assume that the photon beam waist radius and electron beam radius are matched, equation (2.6) can be rewritten as

$$\frac{g_o L_w}{I} = 1.142 \times 10^{-2} \beta \left(\frac{a_w Z_R q}{\lambda_w}\right)^2 \left(\frac{1}{(1+a_w^2)}\right) \left(\frac{q}{\gamma}\right)/\text{amp} \quad (2.7)$$

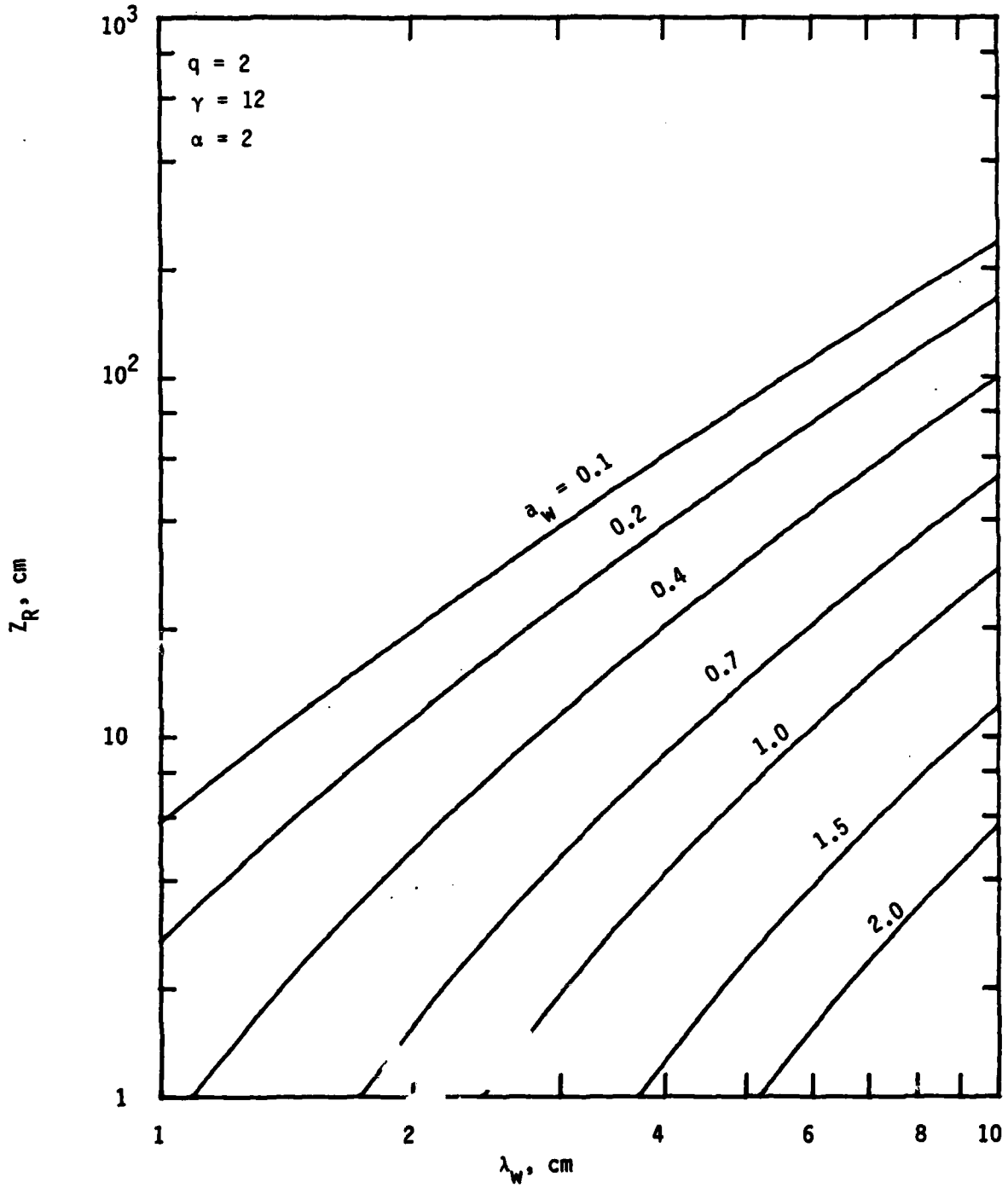

Figure 2. Map of Constant a_w Lines

where I is the total electron beam current and $\beta = v/c$. Once again, this equation differs slightly from eq. (4.7) of Ref. 2 which is incorrect. The saturation flux for a constant parameter wiggler is given by

$$\phi_{sat} \simeq 2.67 \times 10^7 \left(\frac{\gamma}{q}\right)^4 \frac{\lambda_w^2}{a_w^2 \, Z_R^4} \qquad (2.8)$$

For a given set of λ_w and Z_R, a_w can be determined from eq. (2.4). Using eqs. (2.7) and (2.8), we can then find the small signal gain and the saturation flux. Figures 3 to 5 show contours of constant $g_o L_w$, ϕ_{sat} and output wavelength plots for q = 1 and q = 2. In all the cases the magnet gap to optical beam diameter at entrance and exit to the wiggler was taken to be equal to 2. For the UCSB experiment, the same electron beam is planned to be used for the second stage also. Thus, if we fix γ at 12 and pick the first stage parameters, the second stage output wavelength is predetermined. These are also indicated in Figure 5. Now we are in a position to specify the parameters for the proposed UCSB two stage experiment. The Van de Graaff generator is expected to provide 10 amperes current. The bandwidth requirement on the pump wave to be a coherent wave for the second stage is that $\Delta\lambda/\lambda \sim 10^{-4}$. The spontaneous emission from the magnetic wiggler is given by [5]

$$\frac{dI(\omega)}{d\Omega} = 2.94 \times 10^{-8} \cdot h\nu_{ev} \cdot i_{ma} \cdot N \text{ watts/ev of bandwidth /ma/milliradian}^2\text{/cm} \qquad (2.9)$$

For a pump wavelength of 230μ and N = 5, the spontaneous intensity within the bandwidth of interest is found to be $\sim 6.7 \times 10^{-8}$ watts/cm^2. One would need ~ 35 exponentiations to get to saturation levels of 10^8 to 10^9 w/cm^2.

In Figure 6 we have plotted, once again, lines of constant gain, cavity flux, output pump wavelength and a_w in the $\lambda_w - Z_R$ plane. For γ=12, the pump wavelength is limited to 230 to 460μ if we stipulate that the output wavelength is in the visible (4000 to 8000 A°). One

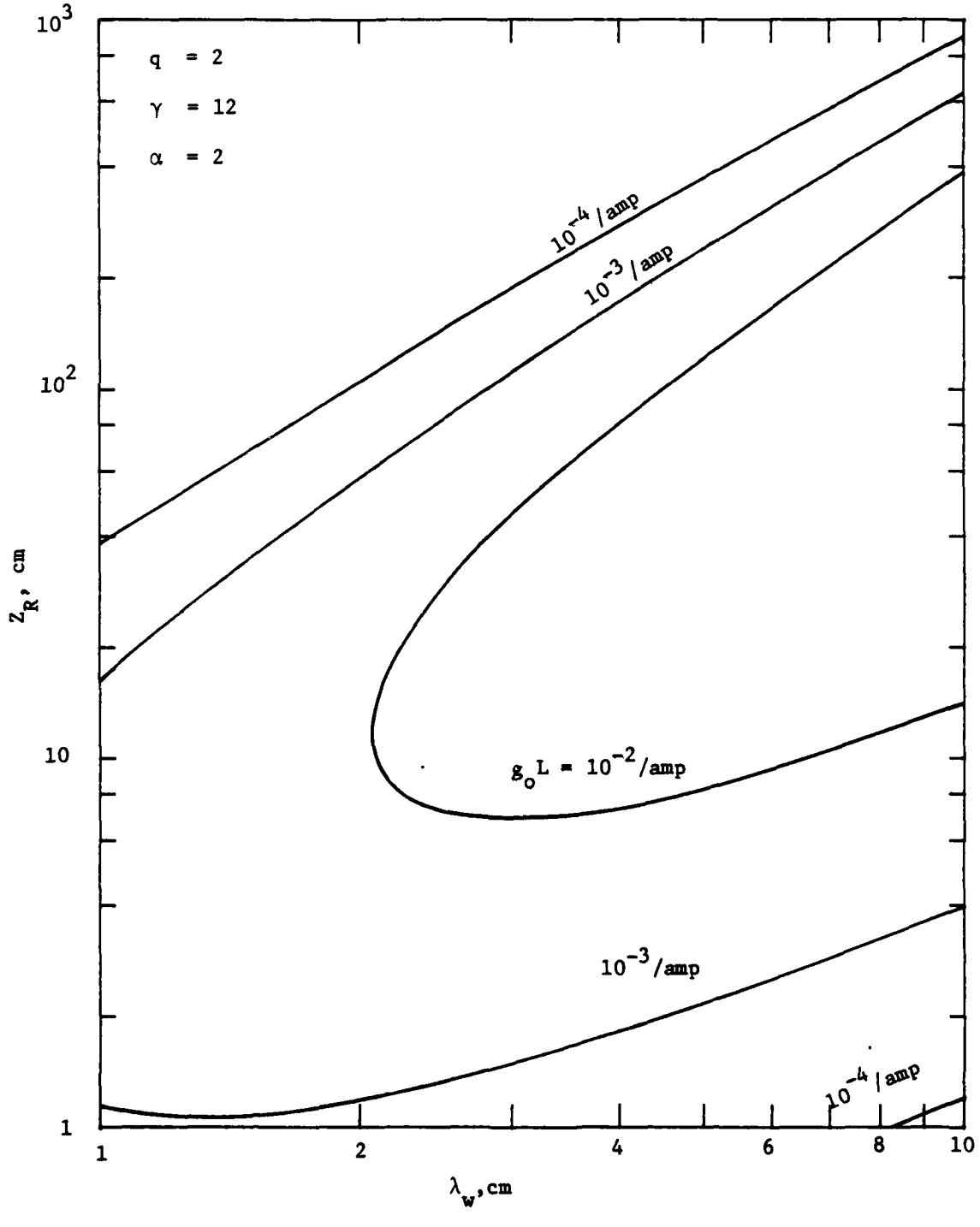

Figure 3. Map of Constant Small Signal Gain Contours for Wiggler Length Equal to Four Times the Rayleigh Range

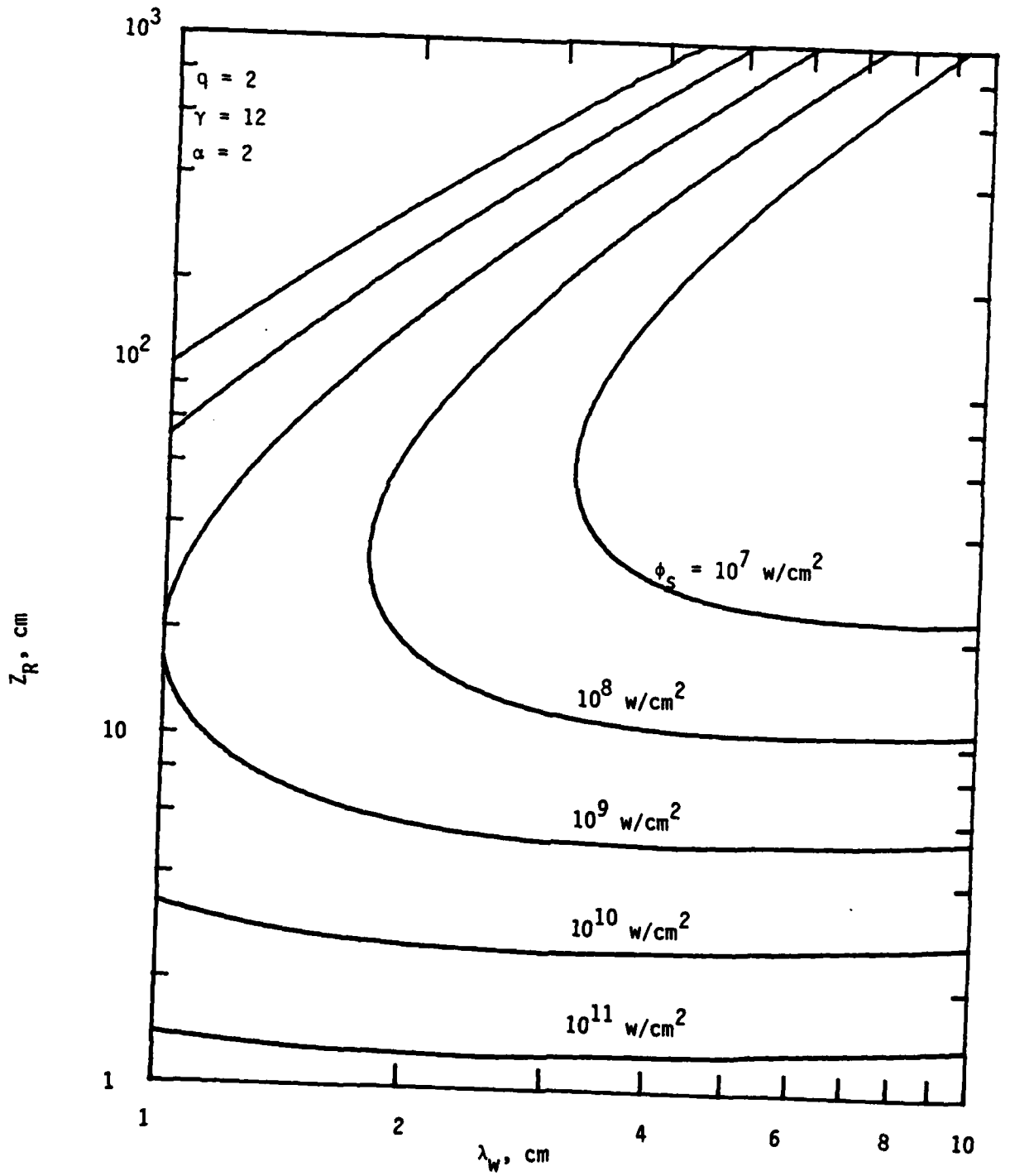

Figure 4. Saturation Flux Contours for $L_w = 4Z_R$

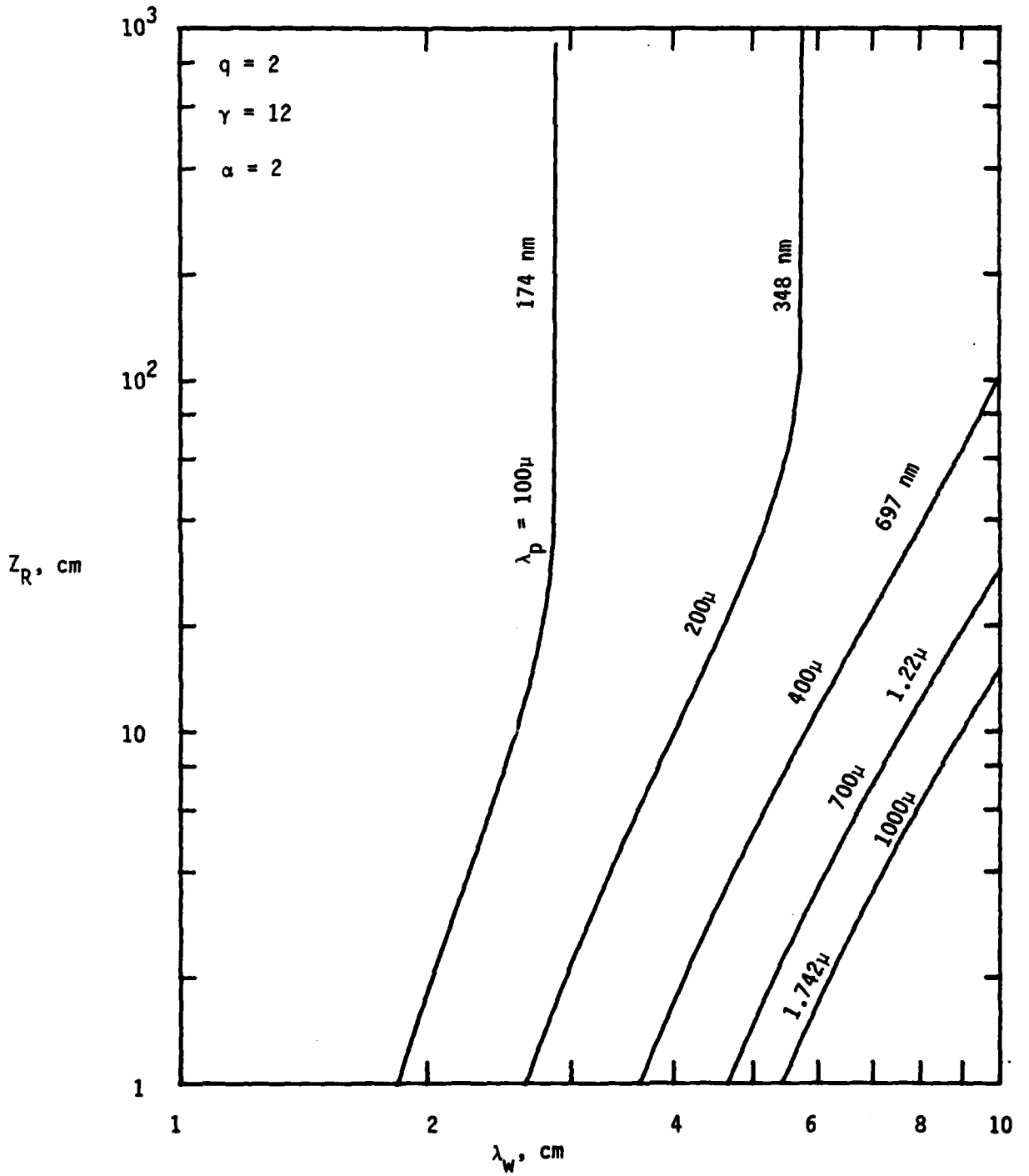

Figure 5. Output Wavelength of the First and Second Stages for $Lw = 4Z_R$

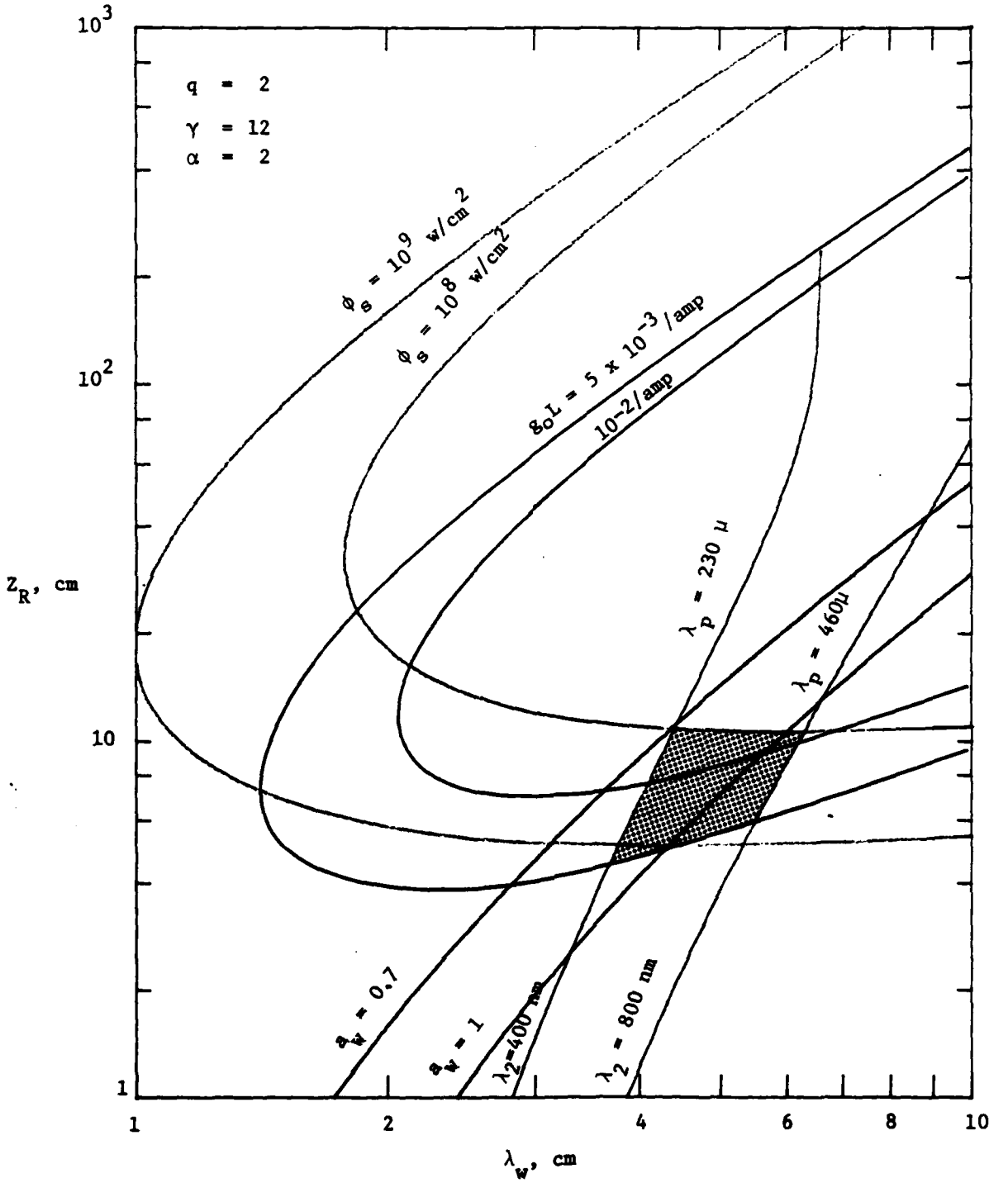

Figure 6. Two-Stage FEL Design Map for γ = 12 and $L_w = 4Z_R$

would also need a small signal gain of at least 5% per pass (requiring ~ 700 passes for saturation). This is important as it directly impacts on the pulse length necessary for a successful two stage operation. From the point of view of wiggler fabrication, one would want to keep $a_w \leq 1$. To achieve reasonable second stage gain, we should have the cavity flux greater than ~ 10^8 w/cm^2. The shaded area in Figure 6 indicates the available parameter space for operation. The actual point that one would pick in this region depends on the pulse length of the electron beam available. If we take the cavity length to be ~ 3 meters, one round trip time is 20 nsec. Thus for 700 passes, the pulse length necessary is 14 μsec. To reduce the pulse length, we have to pick an operating point with higher small signal gain at the expense of decreasing saturation flux. This would reduce the second stage gain and so we cannot arbitrarily increase the small signal gain. We can, however, locate the first stage interaction region away from the beam waist and hope to operate the second stage interaction region at the beam waist. Usually, the advantage gained by such tricks is not overwhelming. If we choose $g_o L_w$ to be 10% per pass (for 10 ampere current), then for a 3 meter cavity, we would need ~ 7 μsec long pulse (neglecting optical losses). A 2 meter cavity would reduce this to ~ 5 μsec. Using Figure 6, we can pick a conceptual design point for the operation of the two stage FEL. It must be borne in mind that the boxed region's boundary is somewhat fuzzy and arbitrary. The requirement on the output wavelength can be considerably relaxed if one uses two separate electron beam sources for the first and second stage. The limit on the minimum gain/amp can be relaxed if the current can be increased to say 100 amperes. For the conceptual design of the two stage FEL, we have chosen the nominal parameter values given in Table I for the UCSB experiment.

For a 10 μsec long pulse, the fluence at the beam waist is ~6 kJ/cm^2. An area expansion of ~ 100 would bring the mirror fluence to 60 J/cm^2 and energy absorbed with 0.2% absorption would be ~ 120

TABLE I

WIGGLER PARAMETERS FOR THE TWO-STAGE FEL EXPERIMENT

γ	=	12
I	=	10 amp
λ_w	=	4 cm
Z_R	=	6 cm
L_W	=	24 cm
a_w	=	0.855
$g_o L_W$	=	7% per pass
ϕ_s	=	5.8×10^8 w/cm^2
ω_o	=	2.14 mm
λ_p	=	240 μ
λ_s	=	419 nm

Number of periods = 6

mj/cm^2, which should be quite safe in terms of mirror damage. If L_c is the length of the optical cavity and R_1 and R_2 are the mirror radii, we can define quantities g_1 and g_2 by

$$g_{1,2} = 1-L/R_{1,2} \qquad (2.10))$$

For stability[6], we require that $0 < g_1 g_2 < 1$. We shall consider the symmetric case with $g_1 = g_2 = g$. Since we want the beam to expand rapidly, we shall choose a design where the cavity is nearly concentric ($L \simeq 2R$).

Let $L/R = 2 - \varepsilon$. Then

$$g = \varepsilon - 1.$$

The radius of the beam at the waist is given by[6]

$$w_o = \left(\frac{\lambda L_c}{\pi}\right)^{1/2} \frac{[g_1 g_2 (1 - g_1 g_2)]^{1/4}}{[g_1 + g_2 - 2g_1 g_2]^{1/2}}$$

$$= \left(\frac{\lambda L_c}{2\pi}\right)^{1/2} \left(\frac{\varepsilon}{2-\varepsilon}\right)^{1/4} \qquad (2.11)$$

Equation (2.11) can be rewritten as

$$\pi w_o^2 = \frac{\lambda Z_R}{2} \frac{L_c}{Z_R} \left(\frac{\varepsilon}{2-\varepsilon}\right)^{1/2} \qquad (2.12)$$

Since Z_R is defined to be $\pi w_o^2/\lambda$, we have,

$$q_c \left[\varepsilon/(2-\varepsilon)\right]^{1/2} = 2 \qquad (2.13)$$

where $q_c = L_c/Z_R$.

The spot size on the mirrors is given by

$$w_1 = \left(\frac{\lambda L_c}{\pi}\right)^{1/2} \left[\frac{g_2}{g_1(1-g_1g_2)}\right]^{1/4} \tag{2.14}$$

This can be cast in the form,

$$q_c \left[\frac{1}{\varepsilon(2-\varepsilon)}\right]^{1/2} = w_1^2/w_0^2 \tag{2.15}$$

From equation (2.13) and (2.15), we obtain,

$$\varepsilon = 2\, w_0^2/w_1^2 \tag{2.16}$$

$$q_c = 2\left(\frac{2-\varepsilon}{\varepsilon}\right)^{1/2} \tag{2.17}$$

Knowing q_c and ε, we can obtain the cavity length and mirror radius of curvature. The diameter of the mirror can be calculated by fixing the diffraction loss. Li[7] has numerically calculated the diffraction losses for different $|g|$ values, and Fresnel numbers. In general, if $|g| < 0.99$, one would need a Fresnel number of 15 or larger to keep the diffraction losses per pass to $< 10^{-4}$. In Table II two different cavity designs are given for an area expansion factor of 100 and 200 for a Fresnel number of 15 ($= a^2/\lambda L_c$, where a is the radius of the mirror).

The choice between the first and second design would depend on other factors such as space to bend the electron beam into and out of the wiggler, electron beam pulse length, etc.

TABLE II

OPTICAL CAVITY PARAMETERS

Beam Area Expansion	100	200
ϵ	0.02	0.01
q_c	19.90	28.21
Cavity Length L_c	119.4 cm	169.3 cm
Radius of Curvature	60.3 cm	85.1 cm
Mirror radius a	6.56 cm	7.81 cm
Pump wavelength	240 μm	240 μm
Cavity Round Trip	~ 8 nsec	~ 11.3 nsec

Having chosen the design values for the wiggler, the single particle electron dynamics code was run to verify the gain and saturation characteristics. The electron dynamics code solves the following two equations:

$$\frac{d}{dt}\ (\gamma\vec{\beta}) = \frac{e}{mc}\ [\vec{E}_r + \vec{\beta} \times (\vec{B}_r + \vec{B}_w)] \qquad (2.18)$$

$$\frac{d}{dt}\ \gamma = \frac{e}{mc}\ \vec{\beta} \cdot \vec{E}_r \qquad (2.19)$$

where $\vec{E}_r$ and $\vec{B}_r$ are the electric and magnetic fields of the radiation and $\vec{B}_w$ is the wiggler field. The equations are solved for different initial phases of the electron with respect to the radiation field and averaged over the initial phase angle.

The results are shown in Figure 7, in which the gain is plotted as a function of the cavity flux for different energy off-sets from the resonant value. Since the energy spread in the incoming electron beam is expected to be less than 0.1%, it is a good approximation to consider the electrons to be monoenergetic. We find the agreement between the exact calculation and the chosen design values to be reasonable.

For a fixed incoming beam energy and wiggler configuration, the wavelength at which maximum gain occurs changes with increasing flux. If there is no wavelength discrimination done by the optical cavity, the output wavelength will progressively shift towards longer wavelength.

The one dimensional calculation described above is correct for only incoming plane waves. It is of interest to study the transverse mode structure under steady state conditions for a given cavity configuration and this is treated in the next chapter.

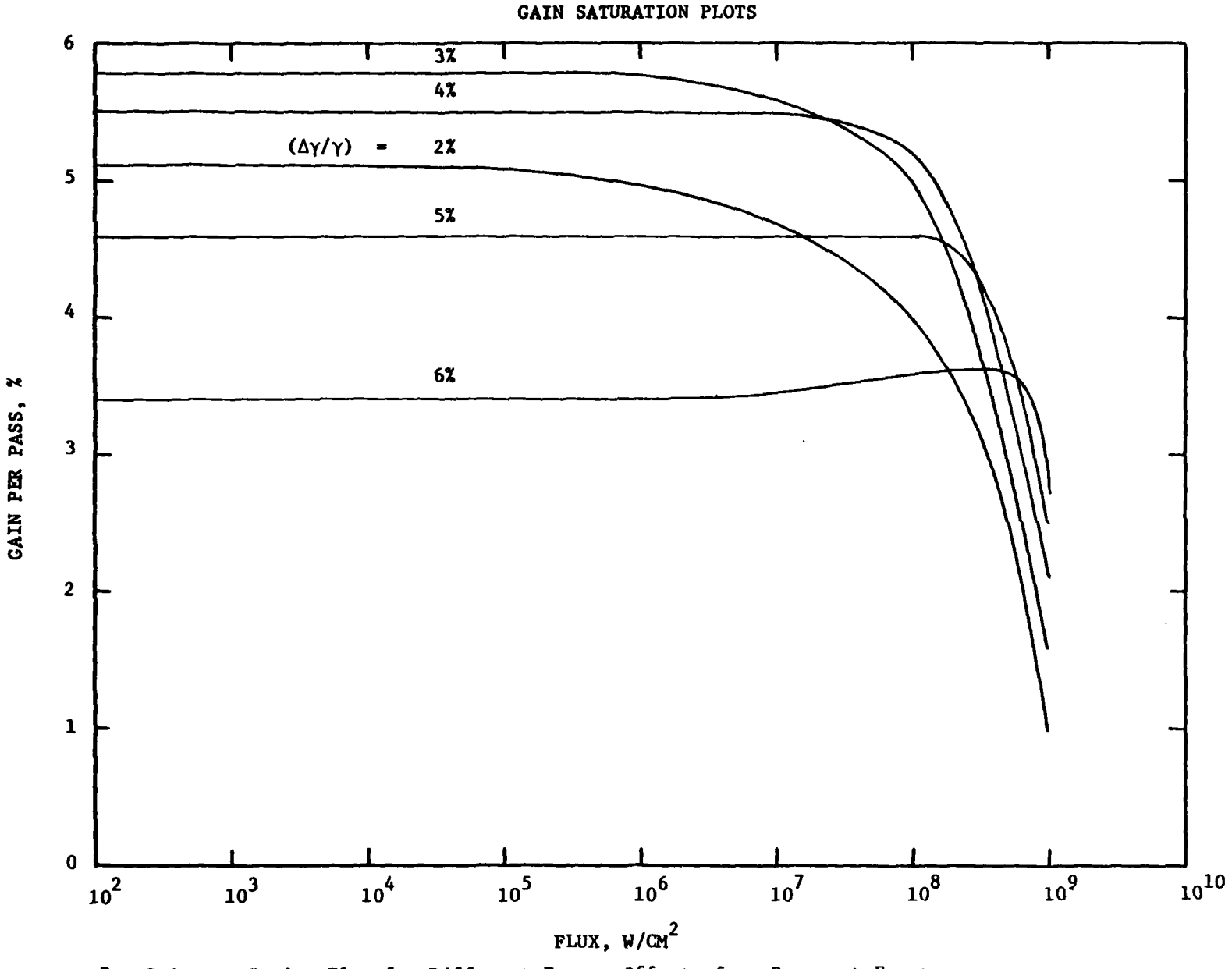

Figure 7. Gain vs. Cavity Flux for Different Energy Offsets from Resonant Energy

III. OPTICAL MODE STRUCTURE

The equations that describe the dynamics of the free electron laser have been given by many authors before[8]. For the sake of consistency in the notation, we follow the work of Kroll, Morton and Rosenbluth[9] and give their derivation below. We assume the wiggler magnetic field and optical field to be derived from the vector potentials

$$\vec{A}_w = \sqrt{2}\,(mc^2/e)a_w(z)\,\hat{x}\,\sin\int_o^z k_w(z_1)dz_1 \tag{3.1}$$

$$\vec{A}_s = \sqrt{2}(mc^2/e)a_s(z)\;\hat{x}\,\sin\int_o^z k_s(z_1)dz_1 - \omega_s t \tag{3.2}$$

where the dimensionless vector potentials $a = eA/mc^2$ have been introduced. We assume that the fractional change in a_w, a_s, k_w and k_s is small over a distance of one period of the wiggler. Maxwell's wave equation for the evolution of the electromagnetic vector potential is given by

$$\frac{\partial^2\vec{A}_s}{\partial z^2} - \frac{1}{c^2}\frac{\partial^2\vec{A}_s}{\partial t^2} = -\frac{4\pi}{c}\vec{J}_\perp\,. \tag{3.3}$$

Writing $k_s(z) = k_{so} + \delta k_s$ and substituting Eq. (3.2) in Eq. (3.3) we obtain

$$\sqrt{2}\left(\frac{mc}{e}\right)^2\left[\frac{2\omega_s}{c}\,\delta k_s\, a_s\,\hat{e}_1 - \frac{2\omega_s}{c}\,a_s'\,\hat{e}_2\right] = \frac{4\pi}{c}\,\vec{J}_\perp, \tag{3.4}$$

where vectors $\hat{e}_1$ and $\hat{e}_2$ are defined by

$$\hat{e}_1 = \hat{x} \sin\left(\int_o^z k_s(z_1)dz_1 - \omega_s t\right) \tag{3.5}$$

$$\hat{e}_2 = \hat{x} \cos\left(\int_o^z k_s(z_1)\, dz_1 - \omega_s t\right) = \hat{e}'_1/k_s \tag{3.6}$$

and we have neglected derivatives of a'_s and δk_s compared to ω_s/c. Because $\hat{e}_1 \cdot \hat{e}_2$ time averages to zero, we find

$$\frac{2\omega_s}{c} \quad \delta k_s A_s = \frac{4\pi}{c} \quad \langle \vec{J}_\perp \cdot \hat{e}_1 \rangle \tag{3.7}$$

where $\langle\ \rangle$ indicates time average.

For a single electron we have

$$\vec{J}_\perp \cdot \hat{e}_1 = e\vec{v}_\perp \cdot \hat{e}_1\ \delta[x-x_o(t)]\delta[y-y_o(t)]\delta[z-z_o(t)] \tag{3.8}$$

where

$$\vec{v}_\perp = \frac{-e\vec{A}}{\gamma mc} \approx \frac{-e\vec{A}_w}{\gamma mc} \tag{3.9}$$

for $A_s \ll A_w$. Hence

$$(\vec{J}_\perp \cdot \hat{e}_1)_{\text{single particle}} = \frac{e^2 A_w(z)}{\gamma mc} \left[\cos\psi - \cos\left(\psi - 2\int_o^z k_w(z_1)dz_1\right)\right]$$

$$\times\ \delta[x-x_o(t)]\delta[y-y_o(t)]\delta[z-z_o(t)] \tag{3.10}$$

where

$$\psi = \int_o^z [k_w(z') + k_s(z')]\, dz' - \omega_s t \tag{3.11}$$

and x_o, y_o and z_o are the coordinates of the electron at time t. Time averaging to remove high frequency variations, summing over all the electrons and averaging over the beam cross-sections, we obtain

$$(\vec{J}_\perp \cdot e_1)_{\text{time average}} = \frac{n_e e^2 A_w}{mc} \left(\frac{\overline{\cos\psi}}{\gamma} \right), \tag{3.12}$$

where n_e is the electron density and $(\overline{\quad})$ means average over initial ψ and energy. Substitution of Eq. (3.12) with Eq. (3.7) yields

$$\delta k_s = \frac{\omega_p^2}{2c\omega_s} \frac{a_w}{a_s} \left(\frac{\overline{\cos\psi}}{\gamma} \right). \tag{3.13}$$

Again from Eq. (3.4), we find

$$\frac{2\omega_s}{c} A_s' = \frac{4\pi}{c} \langle \vec{J}_\perp \cdot e_2 \rangle , \tag{3.14}$$

and proceeding in a similar manner, we find

$$a_s' = \frac{\omega_p^2}{2c\omega_s} a_w \left(\frac{\overline{i_\perp \psi}}{\gamma} \right) \tag{3.15}$$

From Eq. (3.15), we easily obtain,

$$\frac{dE_s}{dz} = 2\pi n_e e a_w \left(\frac{\overline{\sin\psi}}{\gamma} \right) = g E_s \tag{3.16}$$

where E_s is the electric field strength of the electromagnetic wave (in.e.s.u.) and g is the gain per cm. We therefore obtain,

$$g = \frac{2\pi}{10} \frac{a_w J}{E_s} \left(\frac{\overline{\sin\psi}}{\gamma} \right) \tag{3.17}$$

where J is the electron beam current density in amperes/cm^2. It is also easy to see that

$$\delta k_s = g \, (\overline{\cos \psi/\gamma}) \, / \, (\overline{\sin \psi/\gamma}) \tag{3.18}$$

We write $E_s = A_o \, u(x,y)$ where $u(x,y)$ is normalized such that $\iint u(x,y) \, u^*(x,y) \, dx \, dy = 1$. From the relation

$$\frac{c}{4\pi} \iint E_s E_s^* \, dx \, dy = P_s = \text{Cavity Power} \tag{3.19}$$

we find

$$A_o = \left(\frac{4\pi \, P_s \times 10^7}{c} \right)^{1/2} \tag{3.20}$$

where P_s is in watts. Equations (3.17) and (3.18) with the help of the above can be combined to give

$$g - i \, \delta k_s = \frac{2\pi}{10} \left(\frac{c}{4\pi P_s \times 10^7} \right)^{1/2} \frac{a_w(z) J(x,y)}{u(x,y)}$$

$$\times \left[(\overline{\sin \psi/\gamma}) - i \, (\overline{\cos \psi/\gamma}) \right] \tag{3.21}$$

Equation (3.21) will be the starting point for the analysis on the resonator mode structure.

Various techniques exist for finding the modes of a bare resonator. One of the first, and most successful of these is the Fox-Li[10] technique, where an arbitrary amplitude fluctuation is propagated numerically between resonator mirrors until an eigenmode is obtained. The usefulness of this technique depends strongly on obtaining a good initial guess for the mode.

Analytic techniques also exist for obtaining the modes of finite-mirror stable resonators. For the infinite symmetric mirror case, the solutions are those of the integral equation

$$u(x,y) = \iint dx'\, dy'\, u(x',y') \exp\left\{ik\left[(x-x')^2 + (y-y')^2\right]/2L - ib\,(x^2+y^2) - ib\,(x'^2+y'^2)\right\} \qquad (3.22)$$

where

$b = k/2R$, R is the radius of curvature of the mirror and L is the separation between the mirrors. If R = L (confocal resonator) then the equation becomes

$$u(\vec{r}) = \int d\vec{r}'\, u(\vec{r}') \exp\left[-ik(\vec{r}.\vec{r}')/L\right] \qquad (3.23)$$

where the integral extends over the aperture of the cavity. The solutions of Eq. (3.23) are the functions which are their own fourier transform. The solutions are the well-known Hermite-Gaussian functions for the infinite aperture. For the case of finite mirrors the solutions are the so called prolate spheroidal wave functions. Away from the mirror edges ($> \sqrt{\lambda L}$), they reduce to the Hermite-Gauss functions. These solutions were first obtained by Boyd and Gordon[11].

The problem at hand is to find the modes of a loaded resonator with a gain profile of the form given by Eq. (3.21). The technique that we use is that of the degenerate perturbation theory. The degenerate perturbation theory treatment is necessary since the eigenvalues of the lowest modes can differ from each other and the fundamental mode by less than that of the matrix element of the perturbation[12]. Basically, we want to take linear combinations of the lowest order modes via matrix methods to find a prototype "unperturbed state." Once this is done, the ordinary perturbation theory can be implemented. The

reason for following the perturbation theoretical approach is that the integrated single-pass gain of the free electron laser is expected to be less than 1, typically 0.2 to 0.5. In cases when the validity of the perturbation theory is questionable, the results of this analysis can be used as the initial guess for Fox-Li analysis.

The geometry of the problem is sketched in Figure 8. We propagate a ray of light from a point $\vec{r}$ in the plane z = 0 through the gain medium to the right mirror, then back to the left mirror and finally back to the point $\vec{r}'$ in the mid-plane z = 0. It is assumed that the electrons move from left to right. It must be borne in mind that the FEL gain is unidirectional. The integral equation for the loaded system involves the propagator between the points $\vec{r}$ and $\vec{r}'$ in the figure. The equation is of the form

$$\gamma_m u_m(x,y) = \int K(\vec{r},\vec{r}')\, u_m(x',y')\, dx'\, dy' \qquad (3.24)$$

where

$$K = K^{(0)} + K^{(1)} = K^{(0)} \exp\left\{ \int_{\vec{r}}^{\vec{r}'} (g - i\,\delta k_s)\, ds \right\} \qquad (3.25)$$

over the path shown, γ_m is the eigenvalue and $K^{(0)}$ is the kernel of the propagator for the bare resonator given in Eq. (3.23). If $\int (g - i\delta k)\, ds \ll 1$,

then $K^{(1)} \approx K^{(0)} \int_{\vec{r}}^{\vec{r}'} (g - i\,\delta k_s)\, ds$. Actually, the approximation is

better than this, since the gain g for the variable parameter FEL is linear rather than exponential. $K^{(0)}$ represents the effects of the ordinary Fresnel propagator and mirror curvature. To simplify the algebra and the notation in what follows, we shall use matrix form and use K interchangeably with the integral operator and the kernel $K(\vec{r},\vec{r}')$. The eigenvalues and the eigenfunctions of the operator $K^{(0)}$ are known (as given by Boyd and Gordon) for a given set of cavity parameters and we take these to be

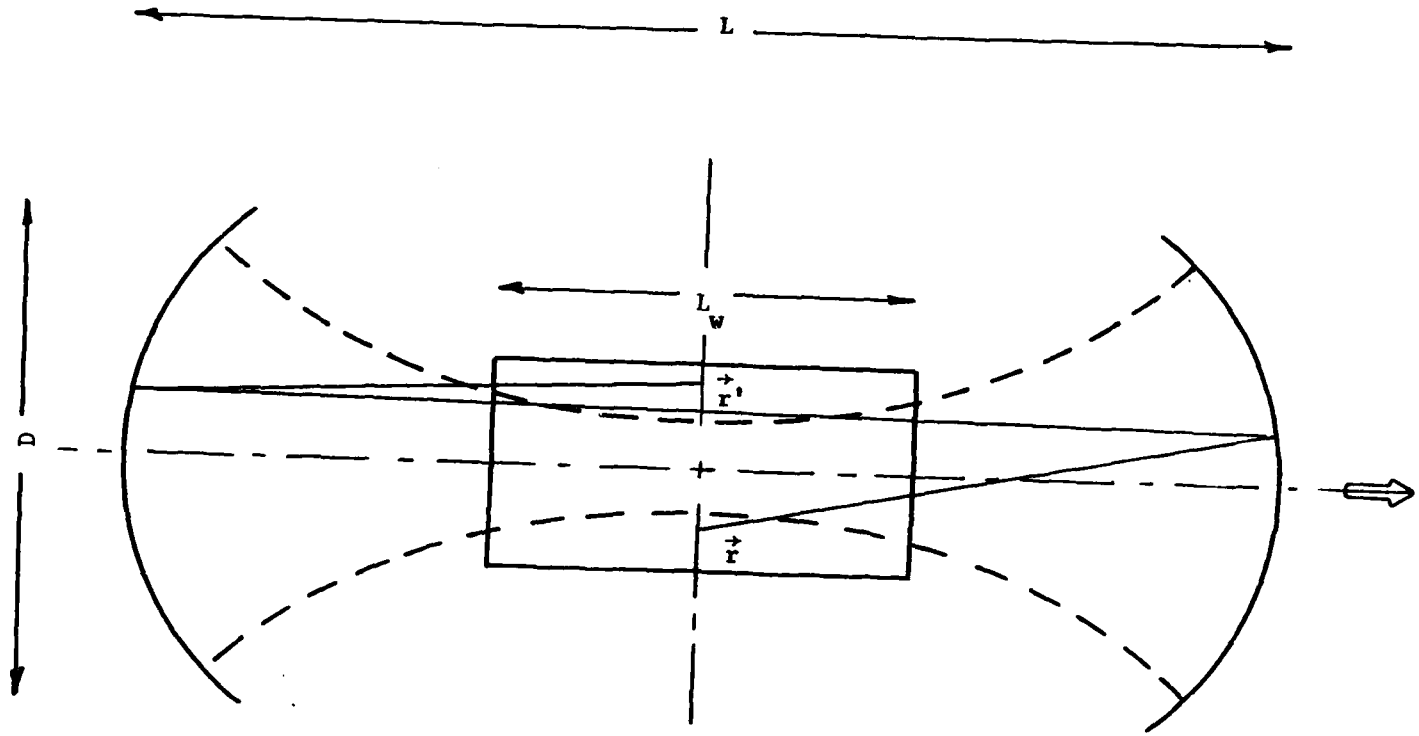

Figure 8. Schematic of the FEL Resonator Illustrating the Path of the Ray from $\vec{r}$ to $\vec{r}'$

$$K^{(0)} u_n^{(0)} = \lambda_n^{(0)} u_n^{(0)} \qquad (3.26)$$

where $u_n^{(0)}$ are the prolate-spheroidal wave functions as mentioned before and $\gamma_n^{(0)}$ are the corresponding eigenvalues. The superscript (0) refers to the order of the solution and the subscript 'n' refers to the n^{th} eigenvalue or eigenfunction. To apply the degenerate perturbation theory, we shall assume s of these eigenvalues to be degenerate or near degenerate. The choice of the eigenfunctions $u_n^{(0)}$ for the degenerate level is usually arbitrary, but ceases to be so if we subject the eigenfunctions to the requirement that the change in them under the action of small applied perturbation be small. Let the correct choice of the new basis of eigenfunctions be of the form $\sum_{m=1}^{s} C_m^{(0)} u_m^{(0)}$.

We write

$$\begin{aligned} K &= K^{(0)} + K^{(1)} + .. \\ u_m &= u_m^{(0)} + u_m^{(1)} + \ldots \\ \gamma_m &= \gamma_m^{(0)} + \gamma_m^{(1)} + \ldots \end{aligned} \qquad (3.27)$$

Straightforward application of the near degenerate perturbation theory yields

$$\sum_n \left[K_{mn}^{(1)} - (\gamma - \gamma_m)^{(0)} \delta_{mn} \right] C_n^{(0)} = 0 \qquad (3.28)$$

where

$$K_{mn}^{(1)} = \iint u_n^{(0)}(x,y)\, K^{(1)}(x,y;\, x',y')\, u_m^{(0)}(x',y')$$

$$dx\, dy\, dx'\, dy' \tag{3.29}$$

For this system of homogeneous linear equations for the quantities $C_n^{(0)}$ to have nontrivial solutions, we require that the secular equation

$$|K_{mn}^{(1)} - (\gamma - \gamma_m^{(0)})\, \delta_{mn}| = 0 \tag{3.30}$$

be satisfied.

Substituting in turn the roots of Eq. (3.30) in the system (3.28) and solving, we find the coefficients $C_n^{(0)}$ and so determine the eignefunction in the zeroth approximation.

The first-order correction to this eigenfunction in the orthogonal space is obtained just as in regular perturbation theory. The coefficients $C_k^{(1)}$, where $k \neq m,n,\ldots$ are obtained as

$$C_k^{(1)} = \frac{\sum_n C_n^{(0)} K_{kn}^{(1)}}{\gamma - \gamma_k^{(0)}} . \tag{3.31}$$

The complete solution correct to first order is given as

$$u_n(x,y) = \sum_{n=1}^{s} C_n^{(0)}\, u_n^{(0)}(x,y)$$

$$+ \sum_{k=s+1}^{\infty} \sum_{n=1}^{s} \frac{C_n^{(0)} K_{kn}^{(1)}}{\gamma - \gamma^{(0)}}\, u_k^{(0)}(x,y) \tag{3.32}$$

For numerical calculations, the series in the second-term is truncated at a convenient point determined by the accuracy of the procedure. This then completes the formal solution to the problem. For the FEL, the matrix element $K_{mn}^{(1)}$ can be written as

$$K_{mn}^{(1)} = \frac{1}{\lambda L} \int dx\, dy\, dx'dy'\, u_m^{(0)}(x,y)\, u_n^{(0)}(x',y')$$
$$\times \exp \{i2b\,[(x'-x_3)^2 + (y'-y_3)^2] - ia\,[x_3^2 + y_3^2]$$
$$+ ib\,[(x_3-x_2)^2 + (y_3-y_2)^2] - ia\,[x_2^2 + y_2^2]$$
$$+ i2b\,[(x_2-x)^2 + (y_2-y)^2]\}\, S(x,y;x',y') \qquad (3.33)$$

where

$$x_2 = (3x+x')/4 \quad , \quad y_2 = (3y+y')/4$$
$$x_3 = (x+3x')/4 \quad , \quad y_3 = (y+3y')/4$$
$$a = \pi/\lambda R \quad , \quad b = \pi/\lambda L.$$

The function S (x,y; x'y') is given by

$$S(x,y;x',y') = \int_{-L_w/2}^{o} dz\, \left[1+\frac{(x-x')^2+(y-y')^2}{4L^2}\right]^{1/2} (g-i\delta k_s)\Big|_{x_1,y_1}$$
$$+ \int_{o}^{L_w/2} dz\, \left[1+\frac{(x-x')^2+(y-y')^2}{4L^2}\right]^{1/2} (g-i\delta k_s)\Big|_{x_2,y_2} \qquad (3.34)$$

where

$$x_1(z) \simeq x' + \left(\frac{x'-x}{2L}\right) z \; ; \; y_1(z) \simeq y' + \left(\frac{y'-y}{2L}\right) z$$

$$x_2(z) \simeq x + \left(\frac{x'-x}{2L}\right) z \; ; \; y_2(z) \simeq y + \left(\frac{y'-y}{2L}\right) z. \qquad (3.35)$$

The electron and photon beam radii at the waist are typically of the order of 1 mm while the mirror-separation may be ~ 1 meter and the wiggler length L_w may be ~ 0.2 meters. We therefore expect z/2L to have a maximum value < 0.25 and one can therefore expand $g(x_1,y_1)$ around $g(x',y')$ in a Taylor series. Similar expansion holds good for $g(x_2,y_2)$. The z-integration can be trivially carried out to the desired order in (L_w/L). The integral in Eq. (3.33) is a four-fold integral which, in general, cannot be reduced to simpler integrals. The numerical evaluation of $K_{mn}^{(1)}$ is probably most conveniently carried out by Monte-Carlo methods. The algebra can be considerably simplified if the gain can be written as a product of separable functions in x and y. The current density J(x,y) in Eq. (3.21) will be taken as Gaussian while for u(x,y) in the same equation, we can take the Gaussian form as the first guess for the solution. This will enable us to break the four-fold integral in Eq. (3.33) to the product of two double integrals which can be conveniently carried out in a computer.

The numerical calculations that have been carried out incorporate further simplifications. The zeroth order eigenfunctions were taken to be Hermite-Gaussian functions rather than the prolate spheroidal functions since the two differ only at the edges of the mirror and the former is easily calculated numerically. It must be emphasized that this simplification is not essential to the method outlined here. Secondly, the zeroth order eigenvalues were calculated approximately by the following means. We first calculate quantities β_m^2 defined by

$$\beta_m^2 = \frac{\int_{-d/2}^{d/2} |H_m(\frac{\sqrt{2}x}{w_1})|^2 \exp[-2x^2/w_1^2]\,dx}{\int_{-\infty}^{\infty} |H_m(\frac{\sqrt{2}x}{w_1})|^2 \exp[-2x^2/w_1^2]\,dx} \qquad (3.36)$$

where w_1 is the beam radius at the mirror. The quantity $\beta_m^2\,\beta_n^2$ gives the fraction of power in the TEM_{mn} modes that is intercepted by the mirror. The eigenfunction $H_m(\frac{\sqrt{2}x}{w_o})\,H_{nen}(\frac{\sqrt{2}y}{w_o})\exp[-(x^2+y^2)/w_o^2]$ represents some k^{th} eigenfunction of the operator $K^{(0)}$ approximately. Hence, we expect $\gamma_k \approx \beta_m\beta_n$. For the numerical example, we take L = 1.2 meters, L_w = 24 cm, and R = 60.3 cm. In Figure 9, we have plotted the intensity profiles on the mirror for different cavity power levels. It is interesting to see that the four lobed distribution, indicative of TEM_{01} and TEM_{10} modes, present at small power levels gives way to a central peaked intensity distribution at high power levels. If we had used circular mirrors and cylindrical coordinates instead of square mirrors and cartesian coordinates, the four-lobed distribution would be replaced by an annular (doughnut shaped) intensity distribution.

For the calculation of the performance of the second stage of the two-stage FEL, it is also of interest to know the intensity distribution at different z-locations in the wiggler. These are shown in Figures 10 to 16 at a cavity power level of 1.44×10^7 watts.

(a) P_c = 14.4 Watts

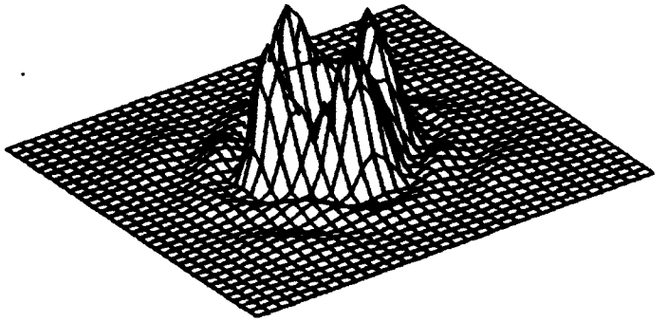

(b) $P_c = 1.44 \times 10^3$ Watts

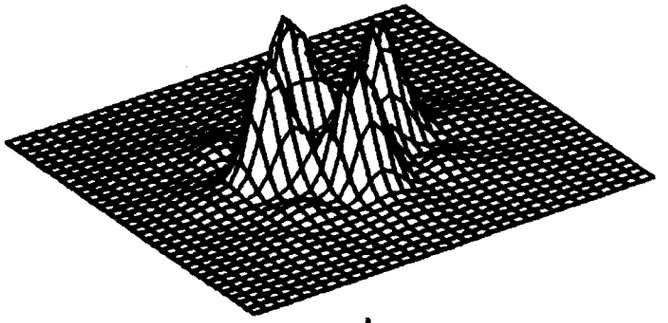

(c) $P_c = 1.44 \times 10^5$ Watts

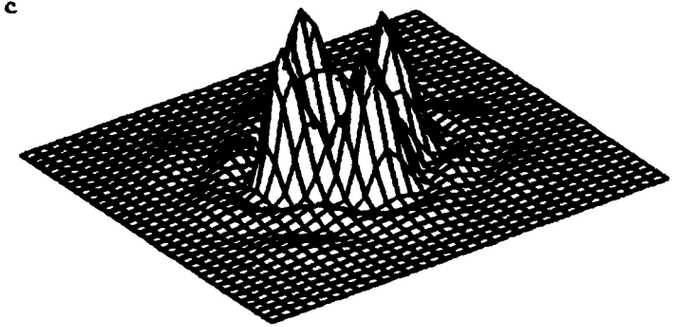

(d) $P_c = 1.44 \times 10^7$ Watts

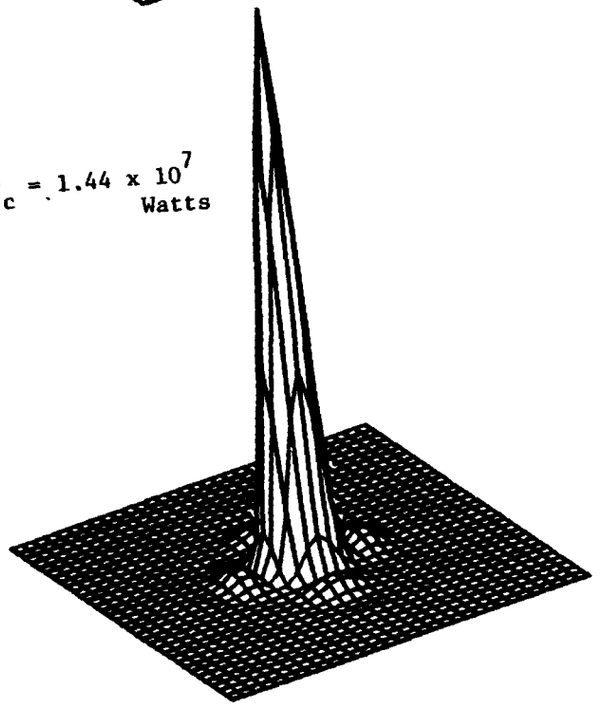

Figure 9. Transverse Intensity Profiles on the Mirror for Different Cavity Power Levels. L_w = 24 cm, L_c = 119.4 cm, R = 60.3 cm, I = 10 amp, λ = 240 μ and Z_R = 6 cm

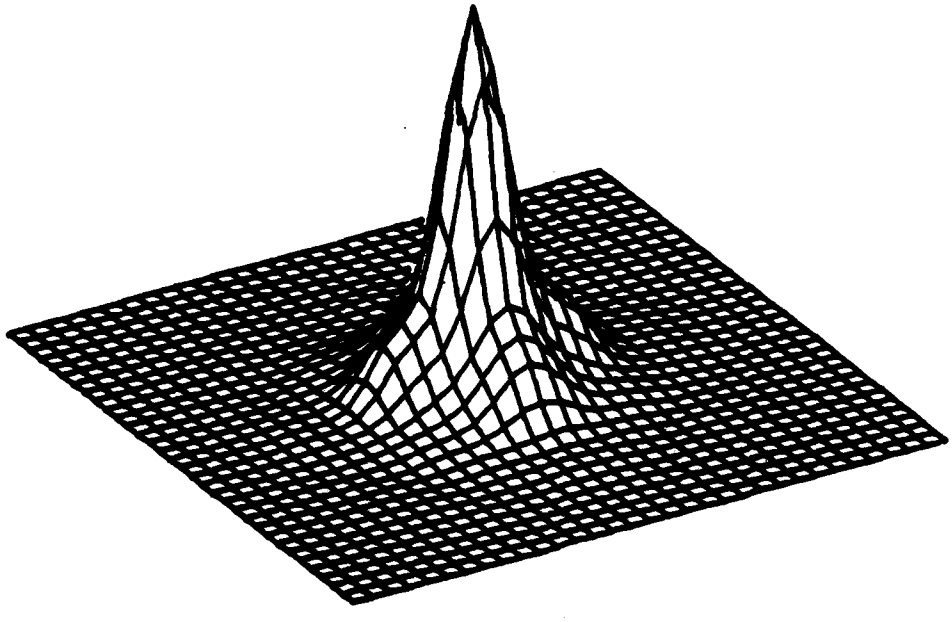

Figure 10. Intensity Distribution of $z = -12$ cm for a Cavity Power Level of 1.44×10^7 watts. Other parameters are the same as in Figure 10. $z = 0$ is the center of the wiggler.

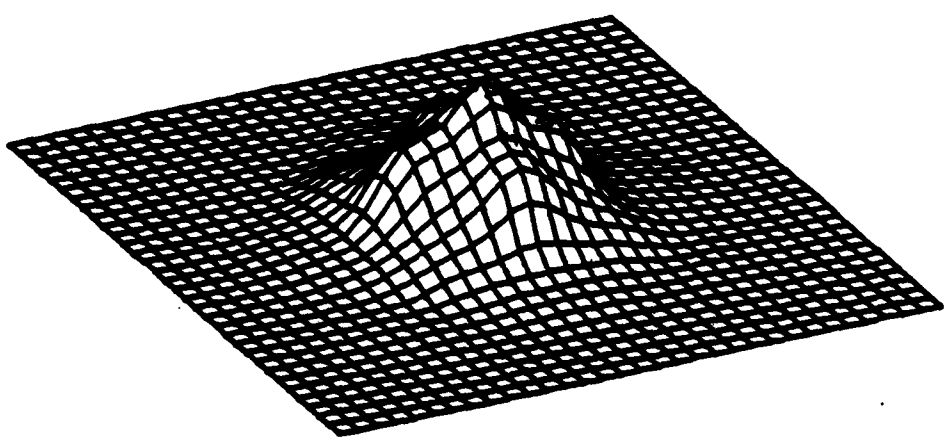

Figure 11. Intensity Distribution at z = -8 cm for the same case as in Figure 10.

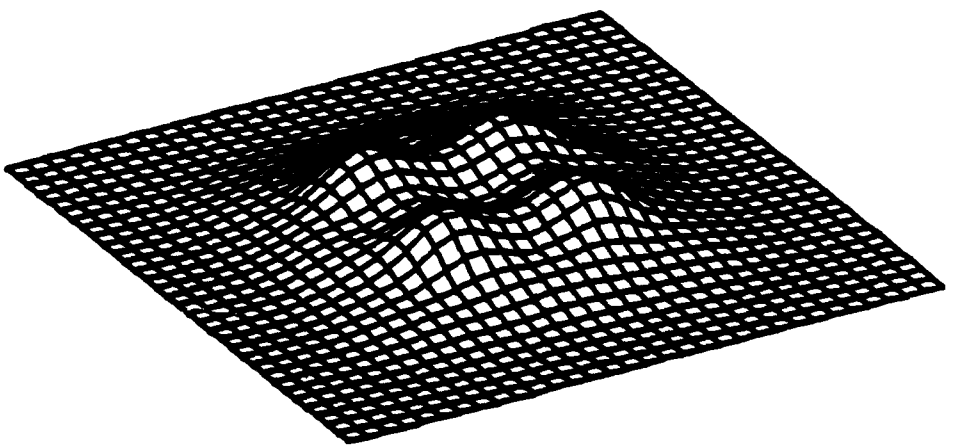

Figure 12. Intensity Distribution at z =-4 cm for the same case as in Figure 10.

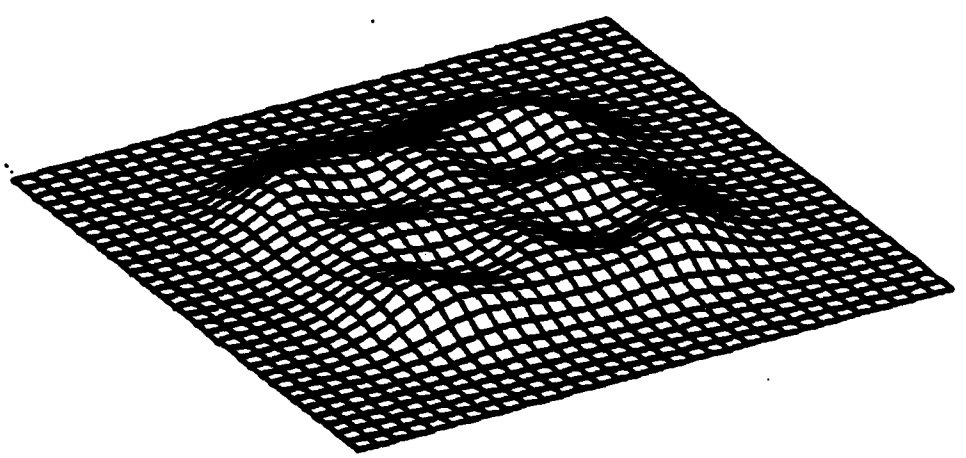

Figure 13. Intensity Distribution at the Center of the Wiggler for the same case as in Figure 10.

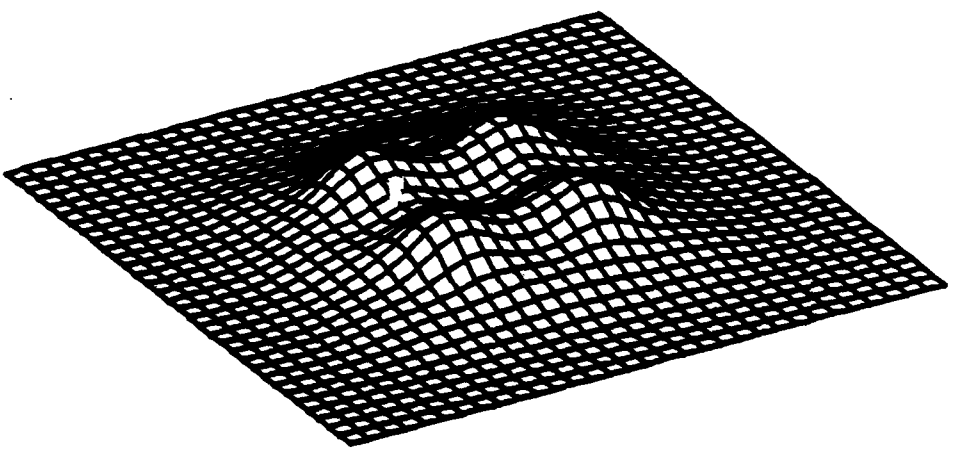

Figure 14. Intensity Distribution at z = + 4 cm for the same case as in Figure 10.

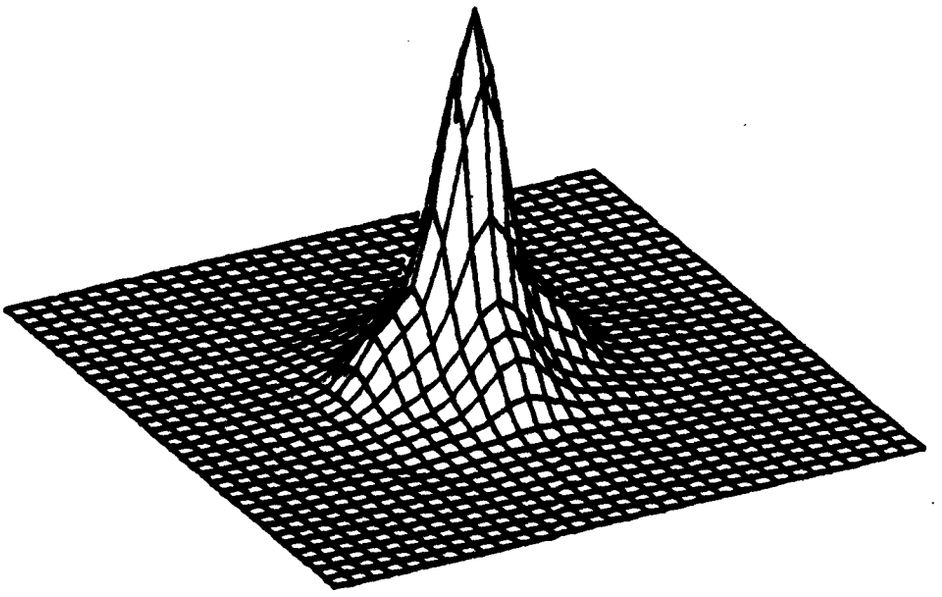

Figure 16. Intensity Distribution at z = 12 cm for the same case as in Figure 10.

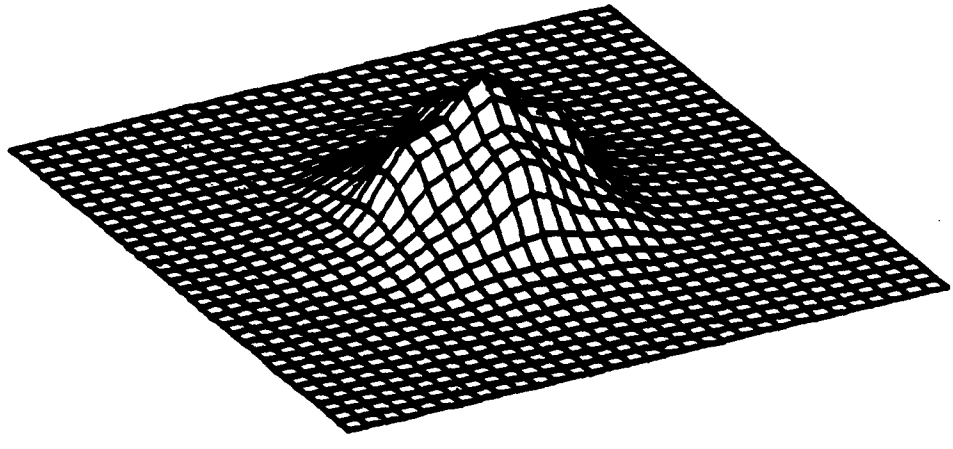

Figure 15. Intensity Distribution at z = + 8 cm for the same case as in Figure 10.

IV. SUMMARY

We have verified the simple conceptual design parameters of the two stage FEL with detailed calculations of electron dynamics. The agreement between the two is quite reasonable. These calculations assume a plane wave propagating through the wiggler. For a given stable cavity configuration, the actual transverse intensity profiles were then calculated using perturbation techniques. The theory used should be accurate for single pass gains less than 50% and for cavity lengths long compared to the wiggler length.

In the continuation of this program, the results of the present calculations will be used to determine the performance of the second stage of the free electron laser that will produce output in the visible portion of the electromagnetic spectrum.

REFERENCES

1. L. R. Elias, Phys. Rev. Lett. 42, 977 (1979).

2. S. A. Mani, "Low Voltage Free Electron Laser Optics," WJSA-FTR-82-193 (March 1982), prepared for Office of Naval Research under contract No. N00014-80-C-0515.

3. TRW Proposal No. 38485-000 R1, "Free Electron Laser Development, Vol. 1, Technical," October 1981, prepared for Office of Naval Research.

4. L. Elias, W. Fairbank, J. Madey, H. A. Schwettman, and T. Smith, Phys. Rev. Letters 36, 717 (1976).

5. B. M. Kincaid, J. Appl. Phys. 48, 2684 (1977).

6. H. Weichell and L. S. Pedrott, Electro-optical Systems Design, July 1976, p. 21.

7. T. Li, Bell System Tech. J. 44, 917 (1965).

8. See for example the articles in "The Physics of Quantum Electronics, Vol. 7" (Addison-Wesley Publishing Company), 1980.

9. N. Kroll, P. Morton, and M. N. Rosenbluth in "The Physics of Quantum Electronics, Vol. 7" (Addison-Wesley Publishing Company, 1980, p. 89.

10. A. G. Fox and T. Li, Bell Syst. Tech. J. 40, 453 (1961).

11. G. D. Boyd and J. P. Gordon, Bell Syst. Tech. J. 40, 489, (1961).

12. See for example L. D. Landau and E. M. Lifshitz, Quantum Mechanics, (Pergamon Press) 1976, p. 133 ff.

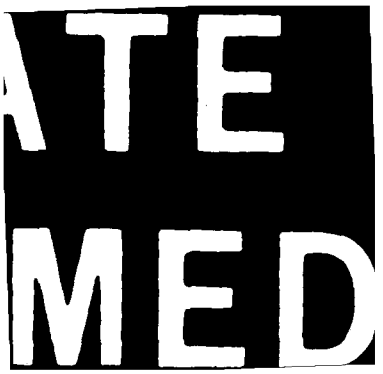
TE
MED